Core losses analysis of the LCL filter inductor for SiC-based inverter

S. Martín-Arroyo[1], D. Cañete[1], J. Herrero Ciudad[2], A. Llamazares[1] and M. García-Gracia[1]

[1] Department of Electrical Engineering
EINA, Zaragoza University
María de Luna 3 – Edificio Torres Quevedo – Campus Río Ebro – 50018 Zaragoza (Spain)
e-mail: **smartin@unizar.es, davidcanete@unizar.es, allamaza@unizar.es, mggracia@unizar.es**

[2] For Optimal Renewable Energy Systems, S.L.
Celsa 17 – Polígono PLA-ZA, 50197 Zaragoza (Spain)
e-mail: **herrero@4fores.es**

Abstract. The ability of SiC devices to switch at high speed allows increasing significantly the power density in both converters and passive components, reducing their required size. To mitigate harmonic injection form inverters into the grid, in order to comply with power quality standards, an accurate filter design is required. Given its excellent performance, an LCL filter is the configuration most suitable in grid-connected power converters. Several parameters must be considered when designing an effective LCL filter, and the inverter-side inductor assumes a special importance because of its relevance to suppress high frequency harmonic content at the inverter side. One of the most relevant issues to be considered in the process of designing the LCL filter is the evaluation of core losses in the inverter-side inductor, which will determine the final temperature of the inductor.

This paper analyses the core losses of the inverter-side inductor of an LCL filter. The proposed method is based on the computation of the current harmonics generated by the inverter and on Steinmetz's empirical equation. As a result, core losses calculated taking into account several carrier and sideband harmonics show good agreement with the experimental values. When current harmonics are estimated by simulation, as it is done in the proposed design procedure, results are less accurate, but precise enough for a design procedure.

Key words. Core losses, LCL filter, SiC inverter, power quality.

1. Introduction

Improving energy and power densities is a major challenge in power inverters. Transport industry (electric vehicle, aircraft, marine, …) as well as domestic and industrial applications require power converters that must be both compact and lightweight. Hence, the achievement of high power density converters is necessary [1]-[2]. Power density can be improved by increasing the switching frequency of the converter [3]. Silicon carbide (SiC) is a semiconductor material suitable for efficient power conversion with higher operating frequency than conventional materials like silicon (Si) [4]-[6].

However, due to the switching frequencies in SiC-based inverters, current harmonics are injected into the grid. The harmonic content must be reduced to ensure compliance with power quality requirements of grid codes. To achieve this, an LCL filter is a common choice in power converters for its excellent performance [7]. Another aspect worth considering is that inductors contribute significantly to the overall weight and volume of converters. Inductors volume can be reduced depending on the maximum flux density that the magnetic material can support without saturating [8]. However, due to low permeability, moderate core loss properties and gradual saturation characteristics of certain core materials, designs can be more limited by temperature rise than by magnetic saturation [9]. Due to the great influence that core losses have on the increase in the temperature of the inverter, its analysis is crucial in order to design an inductor with the lowest possible core losses.

This paper analyses the accuracy in the estimation of core losses by using Steinmetz's equation based on the Fourier expansion of the inductor current, comparing them with the experimental measurements in the inverter-side inductor of the LCL filter in a 20-kW SiC inverter.

2. Design of the inverter-side inductor of the LCL filter

A Metglas (amorphous iron alloy) core has been selected for the side-inverter inductor (Fig. 1) due to its high power density. For the grid-side inductor, an iron core is preferred due to its high saturation flux density and low costs.
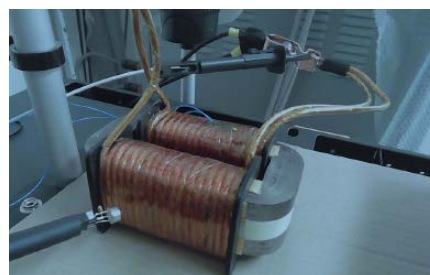

Fig. 1. The inverter-side inductor of the SiC inverter filter.

Fig. 2 shows the current harmonic content for the designed 20 kW, 25 kHz SiC inverter. Firstly, it can be noticed that baseband harmonics are low; secondly, higher harmonics are around the switching frequency and its multiples. Moreover, for a maximum current ripple of 20% on the inverter side, the inductance is inversely proportional to the frequency [10]-[11].
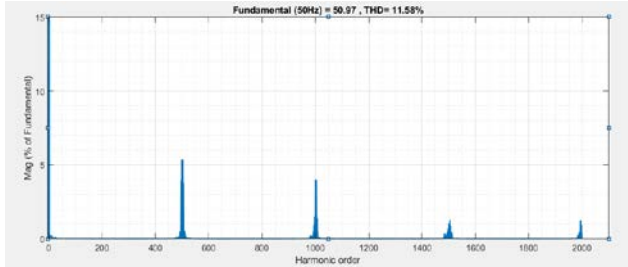

Fig. 2 Current harmonic content.

The losses generated in the winding P_w and in the core P_c increase the inductor temperature. The temperature rise ΔT is expressed as

$$\Delta T = (P_w + P_c) \cdot R_{th} \qquad (1)$$

where R_{th} is the total thermal resistance of the inductor. R_{th} includes [12]:
- the thermal resistance between the core and the ambient
- the thermal resistance between the conductor and the ambient
- the conduction thermal resistance of the conductor and the radiation thermal resistance between the conductor surface and the core.

The inverter-side inductor losses are one of the main contributions to the total filter losses; therefore, their precise evaluation is required in the filter design process.

3. Core losses analysis

A. Classical eddy current and hysteresis losses

To improve inductor size, efficiency and transient response, low inductance values (limited by the maximum current ripple) for the inverter-side are preferred. Core losses increase temperature [13], which is usually the main limitation in high-frequency applications.

The power loss density in the core of the inductor is due to both phenomena, hysteresis and eddy currents.

On the one hand, hysteresis losses are due to the magnetization and demagnetization of the core as alternating current flows, which is caused by the resistance of the molecules in the core to be moved. The instantaneous power delivered to an inductor over one full cycle $p(t)$ is the multiplication of the voltage $v_L(t)$ by the current $i_L(t)$

$$p(t) = v_L(t) \cdot i_L(t) \qquad (2)$$

The energy E_h supplied to the inductor during a period T is

$$E_h = \int_0^T i_L \, v_L dt = N \cdot S \oint i_L dB$$
$$= S \cdot \ell \oint H dB \qquad (3)$$

where B is the magnetic flux density, H the magnetic field intensity, N the number of turns in the coil, S the cross-sectional area and ℓ the core length.

Therefore, the hysteresis power loss density is given by

$$P_h = \frac{E_h}{T \cdot V} = f \cdot \oint H dB \qquad (4)$$

where $V = S \cdot \ell$ is the core volume and f the frequency.

P_h is proportional to the area enclosed by the B-H curve and the frequency

$$P_h = K_h \cdot f \cdot B_m^{\,2} \qquad (5)$$

where K_h is the hysteresis loss coefficient and B_m the flux density amplitude.

According to Faraday's law and Lenz's law, a varying magnetic field causes eddy current to flow in a closed loop, perpendicular to the magnetic field.

Eddy currents in the magnetic core can be expressed in terms of the core material K_e, the frequency and the peak value of the magnetic field as follows

$$P_e = K_e \cdot f^2 \cdot B_m^{\,2} \qquad (6)$$

B. Losses in gapped cores

Power loss in a gapped core is lower than that in the ungapped core with the same magnetic flux density B_m. In that case, the core material power loss density (mW/cm^3) due to both phenomena, hysteresis and eddy currents, can be described by the Steinmetz's empirical equation [14]

$$P_f = k \cdot f^{\mathrm{a}} \cdot B_m^{\,\mathrm{b}} = k \cdot f^{\mathrm{a}} \cdot \left(\frac{\mu_0 N I}{\ell_g + \dfrac{\ell}{\mu_r}} \right)^{\mathrm{b}} \qquad (7)$$

where I (A) is the amplitude of the sinusoidal inductor current, $\ell_g (mm)$ the gap length, μ_r the relative permeability, μ_0 the permittivity of free space, k, a, and b are constants for a given core material at the frequency f (kHz) of the sinusoidal waveform.

However, given that the inductor is used to filter harmonics, the core material power loss density can be estimated by using Fourier expansion of the inductor current

$$P_c = \sum_{j=1}^{\infty} k_j \cdot \left(f_j\right)^{a_j} \cdot \left(\frac{\mu_0 N I_j}{\ell_g + \dfrac{\ell}{\mu_r}}\right)^{b_j} \qquad (8)$$

In the case of the considered amorphous core, μ_r remains constant up to 300 kHz. However, at higher frequencies, there is a dependency of μ_r on frequency. Thereby, at high frequency μ_r becomes complex as is shown in Fig. 3.
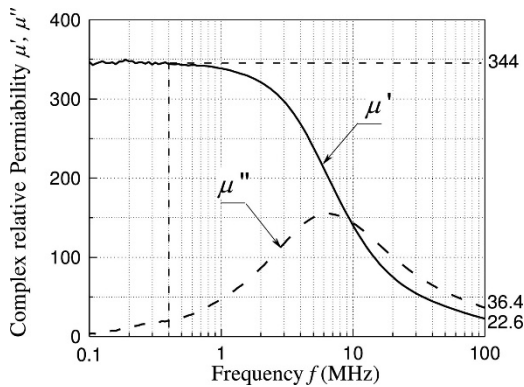

Fig. 3. Complex relative permeability *vs* frequency of the amorphous core [12].

Moreover, the relationship between the flux density, *B* and the magnetic field strength, *H* is given by the permeability which depends on *B*.

$$B = \mu(B) \cdot H \qquad (9)$$

Therefore, the inductance of an inductor depends on the current through the coil or the magnetic flux through the coil.

C. Inductance characterization

The inductance of the designed inductor has been experimentally characterized versus frequency (Fig. 4) and versus the current through the inductor (Fig. 5).
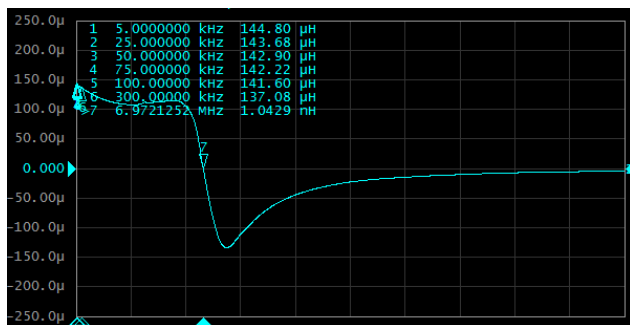

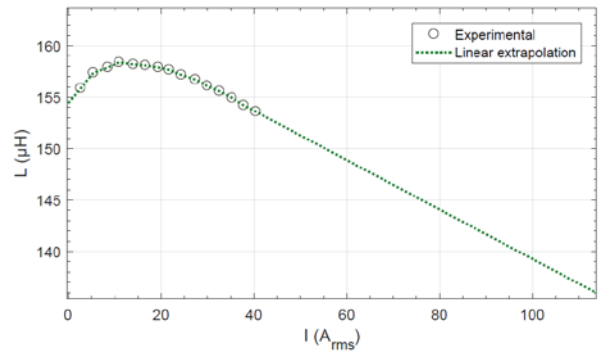Fig. 4. Measurement with VNA (Vector Network Analyzer) of inductance *vs* frequency of the Metglas core.

Fig. 5. Measurement of inductance *vs* current through the inductor.

D. Experimental set up

The experimental set up consist of a 20-kW SiC inverter (Fig. 6) [15], an LCL filter and a 5.57 kW load. The parallel capacitor has a capacitance of 3 µF and a 2.5 Ω series resistor is added to avoid resonance effects. Finally, a three-phase 1 mH grid-side inductor is used.

Fig. 6. SiC inverter test at 20 kHz and 20 kW.

Three single-phase inductors are used in the inverter side (L_1), whose description is given above. To avoid core saturation, a small air gap is placed between two U-cores. Table I shows the key physical characteristics of the designed inductor.

Table I. – Key physical characteristics of the designed inductor (L_1).

Turns	18	-
Magnetic path length	0.292	m
Air gap length	0.002	m
Cross-sectional area	0.000545	m^2
Inductor core mass	1.116	kg

E. Losses in the inductor core

Inverter-side inductor losses have been measured and compared with those calculated using Steinmetz's equation based on the Fourier expansion of the inductor current.

Theoretical results have been compared with experimental results obtained in inductor L_1 of the SiC inverter shown in Fig. 6.

As it can be noticed in Table II, the experimental values measured in L_1 are compared with the results obtained by using (8), considering different number of harmonics. If only the first carrier and sideband harmonics (first 511 current harmonics) are considered, the error is unacceptable (73.6%). When the 5000 current harmonics are considered, the result become close to the measured value (error = 0.6%). However, the experimental results include all losses and, therefore, calculated losses in the conductor must include Litz wire losses [16], in that case a 6.6 % error is obtained.

Table II. – Comparison between the experimental losses measured in L_1 and the results obtained using (8), considering different number of harmonics.

	LOSSES (W)	ERROR (%)
Using (8) and I_j calculated by simulation with 511 first current harmonics (25.55 kHz)	17.2	73.6%
Using (8) and I_j calculated by simulation with 5000 current harmonics (250 kHz)	65.6	0.6%
Using (8) and I_j calculated by simulation with 5000 current harmonics and including Litz wire losses	69.5	6.6%
Experimental value	65.2	-

From the point of view of the inductor design, it may be more helpful to quantify the error when core losses are obtained from current harmonics calculated by simulation. In this way, and under different assumptions, Table III compares the experimentally measured losses with those values calculated using (8) from simulated harmonics. As it can be noticed, the estimated losses are higher (40% error) than the measured value. On the one hand, the simulated (THD = 55.71% before L_1) and experimental (THD = 47.8% before L_1) harmonic content are not the same. On the other hand, in Simulink simulations the resistance of the inductor is considered constant, while there is a strong frequency dependence, as shown in Fig.7.

Table III. – Comparison of experimental losses to those calculated by using (8) from current harmonics obtained through simulation.

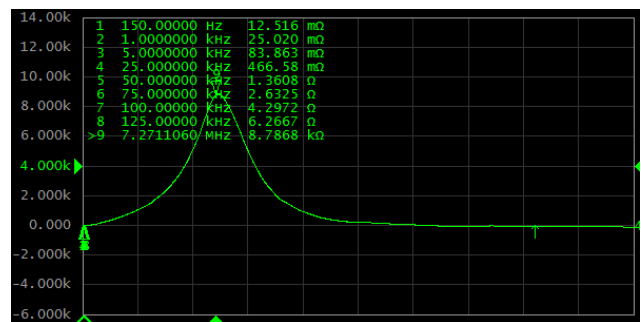|	LOSSES (W)	ERROR (%)
Using (8) and I_j calculated by simulation with 511 first current harmonics (25.55 kHz)	22.1	66%
Using (8) and I_j calculated by simulation with 5000 current harmonics (250 kHz)	87.2	34%
Using (8) and I_j calculated by simulation with 5000 current harmonics and including Litz wire losses	91.1	40%
Experimental value	65.2	-

Fig. 7. Frequency dependence of the resistance of L_1.

In addition, the SiC inverter characterization at this load level gives 66.9 W of losses. The power dissipated in the inverter-side inductor (L_1) (65.2 W) is mainly due to high frequencies, since losses at 50 Hz are only 0.9 W. Fig. 8 shows the measured voltages at both sides of L_1.
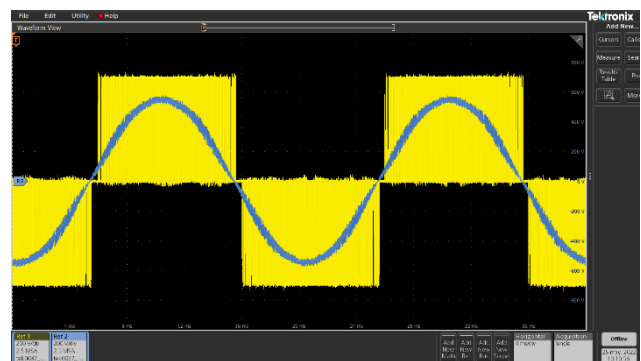

Fig. 8. Experimental voltages in L_1 (voltage in the inverter-side in yellow, voltage in the grid-side in blue).

In the same way, measured losses in the RC branch (R = 2.5 Ω and C = 3 μF) are 108 W; however only 0.34 W are the losses at 50 Hz. Finally, in the grid-side inductor losses are equal to 51 W.

Conclusions

Losses have been measured in the components of a 20-kW SiC inverter. Results confirm that the inverter-side inductor of the LCL filter, together with the RC parallel branch, are essential to suppress higher frequency harmonic content.

A good estimation of core losses in the inverter-side inductor is a relevant parameter in the LCL filter design. Core losses are calculated using (8), Steinmetz's equation based on the Fourier expansion of the inductor current. Results (Table II) obtained using (8) considering different number of harmonics have been compared to the measured core losses. When all carrier and sideband harmonics (5000 current harmonics) are considered, the error is equal to 6.6%.

To check the core losses in the inverter-side inductor in the LCL filter design, experimental losses have been compared (Table III) with those values calculated using (8) from simulated harmonics. In this case, the estimated losses are higher than the measured values, with an error of about 40%, which is totally acceptable.

Acknowledgement

References

[1] A. Voldoire, J.-L. Schanen, J.-P. Ferrieux, A. Derbey and C. Gautier, "Three-Phase PWM Voltage-Source-Inverter Weight Optimization for Aircraft Application Using Deterministic Algorithm", Electronics (2020). Vol. 9 (9). doi: 10.3390/electronics9091393.

[2] X. Zhang, "Passive component weight reduction for three phase power converters", (2014), [Online], Available: https://vtechworks.lib.vt.edu/handle/10919/47788.

[3] P. C. Bolsi, H. C. Sartori and J. R. Pinheiro, "Comparison of Core Technologies Applied to Power Inductors", 13th IEEE International Conference on Industry Applications (INDUSCON) (2018). pp. 1100-1106. doi: 10.1109/INDUSCON.2018.8627236.

[4] J. Hu, O. Alatise, J. A. Ortiz, R. Bonyadi, P. Alexakis, L. Ran and P. Mowby, "Robustness and Balancing of Parallel-Connected Power Devices: SiC Versus CoolMOS", IEEE Transactions On Industrial Electronics (2016). Vol. 63 (4), pp. 2092-2102. doi: 10.1109/TIE.2015.2500187.

[5] Y. Xiong, A. Oyane, T. Ou, S. Thilak, J. Imaoka and M. Yamamoto, "Comparison of switching performance between GaN and SiC MOSFET via 13. 56MHz Half-bridge Inverter", IEEE 29th International Symposium on Industrial Electronics (ISIE) (2020). pp. 672-676. doi: 10.1109/ISIE45063.2020.9152253.

[6] C. Langpoklakpam, A.-C. Liu, K.-H. Chu, L.-H. Hsu, W.-C. Lee, S.-C. Chen, C.-W. Sun, M.-H. Shih, K.-Y. Lee and H.-C. Kuo, "Review of Silicon Carbide Processing for Power MOSFET", Crystals (2022). Vol. 12 (2), 245. doi: 10.3390/cryst12020245.

[7] Y. Liu, "Filter design of high power density converter with weight, size and thermal considerations", Doctoral thesis, Nanyang Technological University, Singapore (2018). [Online], Available: https://dr.ntu.edu.sg/handle/10356/74087.

[8] H. C. Sartori, J. E. Baggio and J. R. Pinheiro, "A comparative design of an optimized boost inductor taking into account three magnetic materials technologies: volume cost and efficiency analysis", 10th IEEE/IAS International Conference on Industry Applications, (2012). pp. 1-6. doi: 10.1109/INDUSCON.2012.6452415.

[9] J. Cox, "Iron Powder Cores for Switchmode Power Supply Inductors", Micrometals Iron Powder Cores, [Online], Available: https://elnamagnetics.com/wp-content/uploads/library/Micrometals/Iron_Powder_Cores_for_Switchmode_Power_Supply_Inductors.pdf.

[10] Y. Liu, K.Y. See, S. Yin, R. Simanjorang, C. F. Tong, A. Nawawi and J.-S. J. Lai, "LCL Filter Design of 50 kW 60 kHz SiC Inverter with Size and Thermal Considerations for Aerospace Applications", IEEE Transactions on Industrial Electronics (2017). Vol. 64 (10), pp. 8321-8333. doi: 10.1109/TIE.2017.2677338.

[11] A. Reznik, M. G. Simoes, A. Al-Durra, and S. M. Muyeen, "LCL Filter design and performance analysis for grid-interconnected systems", IEEE Trans. Ind. Appl. (2014). Doi: 10.1109/TIA.2013.2274612.

[12] M. Tanaka, K. Shimura, M. Sato, T. Mizuno, and T. Matsuoka, "Hybrid inductor for improving gain attenuation characteristics of a Pi filter circuit", Energy Reports (2020). Vol. 6 (9), pp. 446-451, doi: 10.1016/j.egyr.2020.11.215.

[13] M. García-Gracia, M. A. Cova, M. T. Villen, and A. Uson, "Novel modular and retractable permanent magnet motor/generator for flywheel applications with reduced iron losses in stand-by mode", IET Renew. Power Gener. (2014), vol. 8, no. 5, pp. 551–557. doi: 10.1049/iet-rpg.2013.0079 https://es.mathworks.com/help/hdlverifier/ug/fpga-in-the-loop-fil-simulation.html (accessed May 13, 2022).

[14] V. C. Valchev and A. Van den Bossche, "Inductors and Transformers for Power Electronics", Pub. Location: Boca Raton, 1st Edition (2005), doi: 10.1201/9781420027280.

[15] S. Martín-Arroyo, J. A. Cebollero, M. García-Gracia, and Á. Llamazares, "Stand-Alone Hybrid Power Plant Based on SiC Solar PV and Wind Inverters with Smart Spinning Reserve Management", Electronics (2021), vol. 10, no. 7, p. 796. doi: 10.3390/electronics10070796.

[16] M. K. Kazimierczuk, H1. Kazimierczuk, M.K. High-Frequency Magnetic Components: Second Edition; (2013), p.173 and p.294; ISBN 9781118717806. doi: 10.1002/9781118717806.